Molecular basis for ubiquitin and ISG15 cross-reactivity in viral ovarian tumor domains

Masato Akutsu, Yu Ye, Satpal Virdee, Jason W. Chin, and David Komander[1]

Medical Research Council Laboratory of Molecular Biology, Hills Road, Cambridge CB2 0QH, United Kingdom

Edited by* J. Wade Harper, Harvard University, Boston, MA 02115, and accepted by the Editorial Board December 7, 2010 (received for review October 12, 2010)

Crimean Congo hemorrhagic fever virus (CCHFV) is a deadly human pathogen that evades innate immune responses by efficiently interfering with antiviral signaling pathways mediated by NF-κB, IRF3, and IFNα/β. These pathways rely on protein ubiquitination for their activation, and one outcome is the modification of proteins with the ubiquitin (Ub)-like modifier interferon-stimulated gene (ISG)15. CCHFV and related viruses encode a deubiquitinase (DUB) of the ovarian tumor (OTU) family, which unlike eukaryotic OTU DUBs also targets ISG15 modifications. Here we characterized the viral OTU domain of CCHFV (vOTU) biochemically and structurally, revealing that it hydrolyzes four out of six tested Ub linkages, but lacks activity against linear and K29-linked Ub chains. vOTU cleaved Ub and ISG15 with similar kinetics, and we were able to understand vOTU cross-reactivity at the molecular level from crystal structures of vOTU in complex with Ub and ISG15. An N-terminal extension in vOTU not present in eukaryotic OTU binds to the hydrophobic Ile44 patch of Ub, which results in a dramatically different Ub orientation compared to a eukaryotic OTU–Ub complex. The C-terminal Ub-like fold of ISG15 (ISG15-C) adopts an equivalent binding orientation. Interestingly, ISG15-C contains an additional second hydrophobic surface that is specifically contacted by vOTU. These subtle differences in Ub/ISG15 binding allowed the design of vOTU variants specific for either Ub or ISG15, which will be useful tools to understand the relative contribution of ubiquitination vs. ISGylation in viral infection. Furthermore, the crystal structures will allow structure-based design of antiviral agents targeting this enzyme.

cell signaling | structural biology | biochemistry | emerging disease

Mammalian cells are protected against viruses by the innate immune system, which is activated by RNA viruses when pattern recognition receptors such as toll-like receptor-3, retinoic acid inducible protein-I (RIG-I), and melanoma differentiation associated gene 5 (MDA5) bind double-stranded viral RNAs (1). This results in recruitment of adaptor proteins (TRIF, MAVS), and assembly of signaling complexes that include E3 ubiquitin ligases (TRAF6, cIAP, TRAF3) and protein kinases (TAK1, IKKβ, TBK1, IKKε), eventually activating the transcription factors nuclear factor κB (NF-κB) and interferon-regulatory factor (IRF)-3 and -7 (1, 2). IRF and NF-κB activity initiates the production of interferon (IFN)-α and IFN-β. Interferon is secreted from cells and acts as an autocrine stimulant, culminating in the transcription of more than 300 interferon-stimulated genes (ISGs). The ISGs comprise enzymes, transcription factors, cytokines, and chemokines, which mount the antiviral response in the infected and neighboring cells (3).

Protein ubiquitination is a key regulatory posttranslational modification during activation of NF-κB and IRF signaling. During ubiquitination, the small protein Ub is covalently attached to Lys residues in substrate proteins. A key feature of Ub is its ability to form eight distinct polymers, and different polyUb chains have different functions in cells (4). Antiviral signaling involves nondegradative polyUb chains linked through K63 of Ub, which serve to activate RIG-I/MAVS (5) and TAK1 (6). Linear polyUb is important in activation of Inhibitor of κB (IκB) kinases (7), and K48-linked polyUb is required to degrade IκB molecules (6). Ubiquitination is reversed by cellular deubiquitinating enzymes (DUBs) that hydrolyze Ub modifications (8). A number of DUBs including the ovarian tumor (OTU) family members A20 and DUBA have been described as specific inhibitors of NF-κB and IRF signaling, respectively (9, 10).

ISG15 is an antiviral Ub-like protein, that modifies cellular and viral proteins upon viral infection by mechanisms analogous to ubiquitination (11). It contains two Ub-like folds in tandem, structurally resembling diUb, but the individual Ubl-folds are only 33% (proximal moiety, ISG15-N) and 30% (distal moiety, ISG15-C) identical to Ub and display different surface features (11, 12). The antiviral mechanisms of ISG15 modification are beginning to emerge (13). Recent data suggest that ISG15 acts as a cotranslational modification that is attached to newly synthesized viral proteins to inhibit their function (14).

Viruses counteract cellular defense mechanisms and directly interfere with these antiviral signaling pathways to silence the innate immune response. For this purpose, viruses introduce effector proteins into cells during infection. Many effectors interfere with ubiquitination events, and several viruses employ DUBs to inhibit NF-κB and IRF activation (15).

Recent work revealed that Crimean Congo hemorrhagic fever virus (CCHFV) and related *Bunyaviridae*, encode an OTU domain DUB (vOTU) that is cross-reactive and targets both Ub and ISG15 modifications (16). CCHFV is of high medical importance, because it infects humans and results in severe hemorrhagic fever with mortality rates ranging from 30–70% (17). The pathogenesis is only poorly described due to the sporadic occurrence of Crimean Congo hemorrhagic fever (CCHF), the requirement for highest biosafety-level (BSL-4) and lack of animal models (17). To date, no vaccine or specific treatment for CCHF infection is available, necessitating the identification and characterization of drugable CCHFV targets. Because known OTU domain family members are Ub-specific, the unique cross-reactivity with ISG15 in viral OTU domains suggests distinct structural features and unique mechanisms of substrate recognition. This may allow the design of antiviral agents that target viral OTUs specifically.

Here, we have characterized the biochemical and structural properties of the CCHFV viral OTU domain (vOTU). Analysis of enzyme kinetics confirmed cross-reactivity. vOTU displayed a unique Ub linkage-specificity profile as it was inefficient in cleaving K29-linked and linear chains. Crystal structures of vOTU and complexes with Ub and ISG15 revealed an N-terminal extension

Author contributions: M.A. and D.K. designed research; M.A., Y.Y., and D.K. performed research; S.V. and J.W.C. contributed new reagents/analytic tools; M.A., Y.Y., and D.K. analyzed data; and D.K. wrote the paper.

Conflict of interest statement: D.K. is a consultant for Ubiquigent, Inc.

This article is a PNAS Direct Submission. J.W.H. is a guest editor invited by the Editorial Board.

Data deposition: The atomic coordinates and structure factors have been deposited in the Protein Data Bank, www.pdb.org [PDB ID codes 3PHU (apo), 3PHW (Ub complex), and 3PHX (ISG15 complex)].

[1]To whom correspondence should be addressed. E-mail: dk@mrc-lmb.cam.ac.uk.

This article contains supporting information online at www.pnas.org/lookup/suppl/doi:10.1073/pnas.1015287108/-/DCSupplemental.

not present in eukaryotic OTU domains, which formed the substrate binding site and induced a different orientation of a bound Ub or ISG15 moiety. The binding surface properties of Ub and ISG15 allowed generation of vOTU point mutants that were specific for only one of the two modifiers. Our studies reveal unique features of vOTU that may be exploited in structure-based inhibitor design. Furthermore, Ub- and ISG15-specific vOTU variants may be useful tools to understand the relative contribution of ubiquitination vs. ISG15 modification in viral pathogenesis.

Results

The N-terminal 169 amino acids (Aa) of the L-protein of CCHFV comprising the OTU domain had previously been shown to be sufficient for deubiquitinase and deISGylase activity (16). Bacterial expression plasmids of a slightly longer fragment (residues 1–217) were obtained by gene synthesis of an *Escherichia coli* codon-optimized cDNA. When this fragment was expressed in bacteria, C-terminal degradation products could be observed, leading to a shorter construct spanning residues 1–183 (referred to as vOTU).

Cross-Reactivity and Linkage-Specificity of vOTU. vOTU was biochemically characterized and its activity against Ub-AMC and ISG15-AMC model substrates was compared in quantitative measurements (Fig. 1 *A* and *B*). Consistent with previous qualitative results (16), this revealed that vOTU acts on both modifiers with similar kinetics, showing a ~2-fold lower K_M for ISG15 compared to Ub (6 μM vs. 13 μM, Fig. 1*C*). Ub can form eight different types of polymers (4), and six different diUb chains have been synthesized in quantities allowing biochemical measurements (4, 18, 19). We tested the chain linkage-specificity of vOTU against K6-, K11-, K29-, K48-, K63-linked, and linear diUb (Fig. 1*D*). vOTU cleaved K6-, K11-, K48-, and K63-linkages, whereas it was inefficient in cleaving K29-linked and linear diUb.

The inefficiency of eukaryotic OTU domains (20, 21) and vOTU of CCHFV (22) to hydrolyze linear chains has been noted previously, and suggests that OTU domains distinguish between isopeptide bonds in Lys-linked polyUb and peptide bonds present in linear chains (20, 22). In Ub-AMC, a bulky fluorescent group is attached via a peptide linkage to the Ub C-terminus, possibly making it a suboptimal substrate for vOTU. We hence tested a recently developed assay based on fluorescence anisotropy (19). In this assay, a K63-linked diUb molecule with a single fluorescent group at the C-terminus of the proximal Ub is cleaved at the isopeptide bond linking the Ub moieties, resulting in fluorescent monoUb. The difference in molecular weight from fluorescent diUb (17 kDa) to fluorescent monoUb (8.5 kDa) can be monitored in anisotropy measurements. This analysis revealed a >10-fold lower K_M (930 nM for K63-diUb compared to 13 μM for Ub-AMC), a 2-fold increased k_{cat} (7.5 compared to 3.7 s^{-1}) and hence a >25-fold higher specificity constant (k_{cat}/K_M, 8.2×10^6 compared to 2.9×10^5 M^{-1} s^{-1}) for vOTU activity against K63-linked diUb compared to Ub-AMC (Fig. 1 *C* and *E*). The kinetic measurements of vOTU activity against K63-linked diUb provide a more physiological estimate for activity, because a natural substrate linked by an isopeptide bond is being used. In addition, the proximal Ub unit not present in Ub-AMC may contribute to higher binding affinity. The significant differences between the Ub-AMC and diUb assay highlight the need for improved quantitative DUB and deISGylase assays. Nevertheless, the data obtained from AMC assays allow a direct comparison between Ub and ISG15, because both activity probes release an identical fluorescent AMC group upon hydrolysis by vOTU.

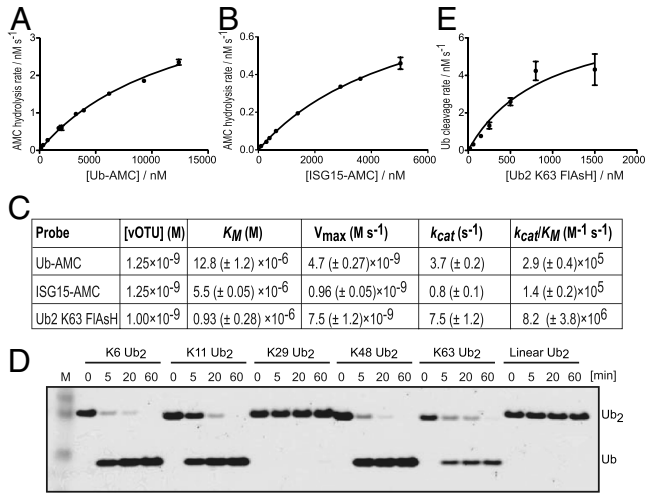

C

Probe	[vOTU] (M)	K_M (M)	V_{max} (M s^{-1})	k_{cat} (s^{-1})	k_{cat}/K_M (M^{-1} s^{-1})
Ub-AMC	1.25×10^{-9}	$12.8 (\pm 1.2) \times10^{-6}$	$4.7 (\pm 0.27)\times10^{-9}$	3.7 (± 0.2)	$2.9 (\pm 0.4)\times10^{5}$
ISG15-AMC	1.25×10^{-9}	$5.5 (\pm 0.05) \times10^{-6}$	$0.96 (\pm 0.05)\times10^{-9}$	0.8 (± 0.1)	$1.4 (\pm 0.2)\times10^{5}$
Ub2 K63 FlAsH	1.00×10^{-9}	$0.93 (\pm 0.28) \times10^{-6}$	$7.5 (\pm 1.2)\times10^{-9}$	7.5 (± 1.2)	$8.2 (\pm 3.8)\times10^{6}$

Fig. 1. Cross-reactivity and linkage specificity of CCHFV vOTU. (*A*) Michaelis–Menten kinetics for vOTU determined by quantitative Ub-AMC measurements. Curve-fitting was performed with GraphPad Prism. (*B*) Michaelis–Menten kinetics determined with ISG15-AMC. (*C*) Table summarizing the kinetic parameters for vOTU. (*D*) Qualitative linkage-specificity analysis of vOTU against diUb of different linkages was performed according to ref. 20. vOTU (2.5 ng) was incubated with 1.5 μg diUb in 30 μL volume at 37 °C. 5 μL samples were taken at indicated time points, resolved on a 4–12% SDS-PAGE gel and silver stained. (*E*) Michaelis–Menten kinetics derived from a fluorescence anisotropy assay against FlAsH-tagged K63-linked diUb.

Structural Analysis of vOTU. Purified vOTU (residues 1–217) was crystallized, and diffraction data to 2.2 Å resolution were collected (Table S1). The structure was determined by single-wavelength anomalous dispersion (SAD) phasing using a crystal grown from SeMet substituted vOTU. Two molecules in the asymmetric unit (AU) were refined to final statistics shown in Table S1. Molecule (mol) A shows contiguous electron density from residues 1–182. Mol B is less well ordered, displaying electron density for residues 8–192, but lacking density in several surface loops. Mol A defined the vOTU domain fold and will be discussed below.

The structure of vOTU domain (Fig. 2*A*) revealed a catalytic domain fold most similar to yeast Otu1 [yOtu1, Protein Data Bank (PDB) ID 3by4 (23), rmsd of 1.82 Å over 115 Aa] (Fig. 2 *B* and *C*). A unique N-terminal extension in vOTU (residues 1–20) extends the central five-stranded β-sheet by two strands. A short upstream helix packs against this extended seven-stranded β-sheet (Fig. 2*A*). This N-terminal extension is absent in yOtu1 (Fig. 2 *B* and *C*) and other eukaryotic OTU domains such as OTUB1, OTUB2, and A20 (Fig. S1). The N-terminal extension is located such that it contributes to the S1 Ub/ISG15 binding site (Fig. 2*A*). The catalytic triad of vOTU consists of Cys40, His151, and Asp153. The triad residues are interacting, forming a catalytic site that is poised for catalysis (Fig 2*A*). In the unliganded structure, the catalytic Cys40 is oxidized to Cys sulphinic acid.

Molecular Basis for Ub- and ISG15 Binding to vOTU. To understand the molecular basis for OTU domain cross-reactivity, we reacted vOTU with suicide inhibitors derived from Ub or ISG15 (24), and determined complex crystal structures of these substrates bound at the S1 site of vOTU (Fig. 3). For this, the Ub or ISG15 C-terminus was exchanged to an electrophilic group that reacted rapidly and quantitatively with the catalytic Cys of vOTU, forming a covalent complex that could be purified and crystallized.

Crystals of vOTU–Ub diffracted to 2.0 Å resolution and contained 4 complexes per AU (Fig. 3*A*). ISG15 contains two Ub-like folds in tandem. Suicide probes generated with full-length ISG15 (ISG15-FL) or the isolated C-terminal Ub-like fold of ISG15 (residues 79–156, ISG15-C), reacted equally well with vOTU suggesting similar affinities. We purified vOTU complexes covalently bound to ISG15-FL and ISG15-C, and were able to determine the structure of vOTU–ISG15-C to 1.6 Å resolution with 1 complex

BIOCHEMISTRY

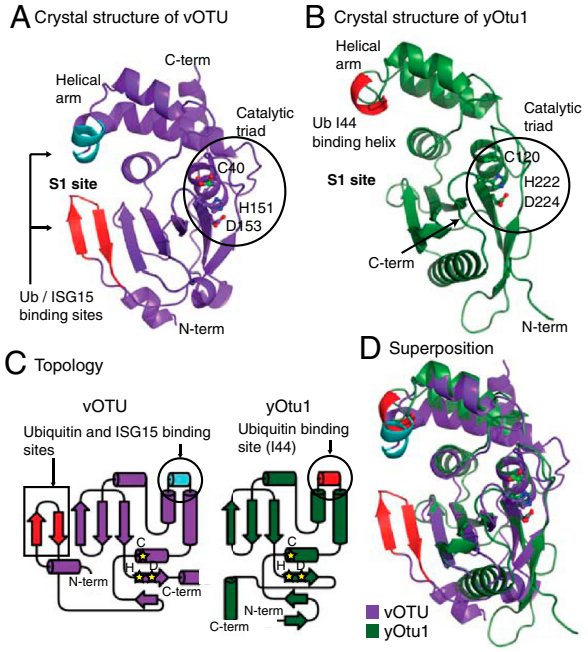

Fig. 2. Structural features of the CCHFV OTU domain. (*A*) Structure of the vOTU domain in cartoon representation. Secondary structure elements facilitating Ub/ISG15 binding are highlighted in orange/green. Catalytic site residues are shown in ball-and-stick representation with residues labeled. All structure figures were prepared with PyMol (www.pymol.org). (*B*) Crystal structure of yOtu1 [green; PDB ID 3by4 (23)]. The Ub contacting helix in the helical arm is coloured orange and catalytic site residues are shown. (*C*) Topology diagrams of vOTU and yOtu1 colored as in A/B. Yellow stars indicate the relative position of catalytic site residues, and Ub/ISG15 interacting regions are indicated. Topology diagrams were prepared with TopDraw. (*D*) Superposition of vOTU (colored as in *A*) and yOtu1 (colored as in *C*).

in the AU (Fig. 3*B*). The vOTU domain superposes well in all determined structures (rmsd up to 0.5 Å), indicating that Ub or ISG15 binding does not induce major conformational changes.

In the complex structures, Ub and ISG15-C occupy identical positions and orientations (Fig. 3 *A* and *B*), and their conserved C-terminal sequences comprising a LRLRGG motif form identical contacts with the catalytic site of vOTU (see electron density inset in Fig. 3 *A* and *B*). A previous crystal structure of free ISG15-FL [PDB ID 1z2m, (12)], can be superposed with its C-terminal Ubl-fold onto ISG15-C in the vOTU complex (Fig. 3*B*). In this model, the N-terminal Ubl-fold does not provide additional interactions with the catalytic core, indicating that ISG15-C provides most if not all of the binding surface.

Structural Detail of the vOTU–Ub Interaction. The vOTU–Ub complex was compared with the previously reported yOtul–Ub complex (23). yOtu1 binds Ub via a helical arm that is structurally conserved in all OTU domains including vOTU (Fig. 2 *B* and *C* and Fig. S1) (8). In yOtul–Ub, a short hydrophobic helix at the tip of the helical arm interacts with the hydrophobic patch of Ub consisting of residues Ile44, Leu8, Val70, and His68 (Fig. 3*C*). Most ubiquitin binding proteins including all DUBs interact with this hydrophobic patch (4, 8).

The orientation of Ub in complex with vOTU is dramatically different compared to yOtul–Ub (Fig. 3*D*). The Ub molecule occupies a similar S1 binding site in vOTU, but the Ub molecule rotates by ~75° compared to yOtul–Ub so that the Ub hydrophobic patch interacts with the unique N-terminal β-strands in vOTU, and not with the helical arm (Fig. 3*A*). The β-strands comprise several exposed and conserved hydrophobic residues, namely Val12, Ile13, and Val18 that interact with the Ub hydrophobic patch. Further polar contacts exist between vOTU Gln16/Ub Arg42, and vOTU Asn20/Ub Gly10 (Fig. S2).

The vOTU helical arm contains Pro77 and Leu81 on a hydrophobic helix close to the Ub molecule. However, due to rotation of Ub, this helix is now adjacent to polar Ub residues, Gln49 and Arg42. One polar interaction between vOTU Glu78 and Arg72 of Ub is formed via this interface (Fig. S2).

Structural Detail of the vOTU–ISG15 Interaction. ISG15-C is 30% identical with Ub, and displays different surface properties when compared with Ub (12). Residues homologous to the hydrophobic patch in Ub are replaced in ISG15-C by polar amino acids; i.e., Thr125 (Ile44 in Ub), Asn151 (Val70), and Asn89 (Leu8) (Fig. 3*B*). However, an exposed nearby aromatic residue, Phe149 (at the His68 position in Ub) preserves a hydrophobic character of this surface in ISG15-C. In complex with vOTU, this hydrophobic surface centered on Phe149 contacts Val12 and Val18 of the vOTU N-terminal extension similarly to the Ub hydrophobic patch (Fig. 3*B*).

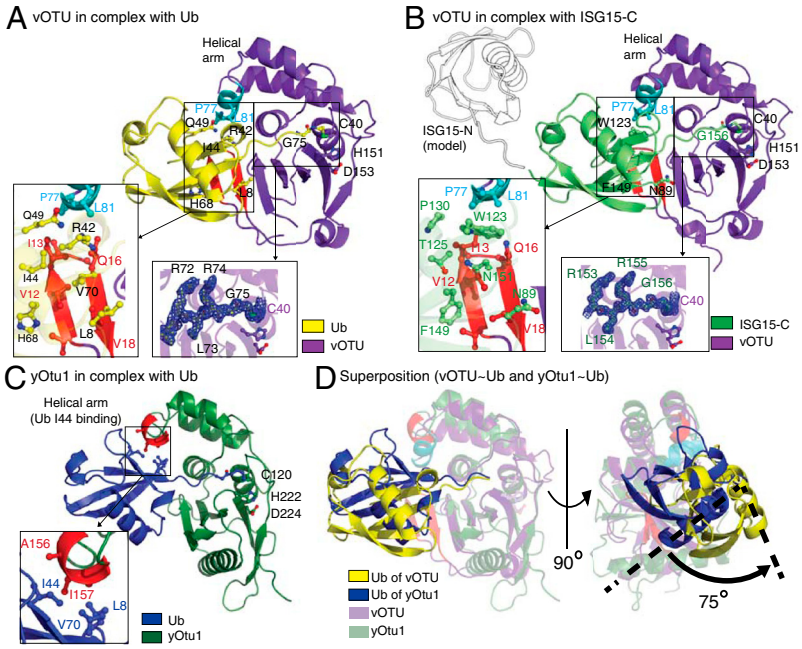

Fig. 3. Structures of vOTU in complex with Ub and ISG15-C. (*A*) Structure of vOTU in complex with Ub. The large picture shows the complex, with the OTU domain labeled as in Fig. 2*A*, and Ub in yellow. Residues mediating the interactions are shown in ball-and-stick representation and labeled. Two insets show the molecular detail of Ub binding to the N-terminal β-sheet (*Left*) and weighted 2|Fo|-|Fc| electron density contoured at 1σ, for the Ub C-terminus linked to the catalytic site Cys residue (*Right*). (*B*) Structure of vOTU in complex with ISG15-C (in green), images according to (*A*). The N-terminal Ubl-fold of ISG15 is modeled (outlined in black) according to the crystal structure of full-length ISG15 [PDB ID 1z2m (12)]. (*C*) Structure of yOtu1 (green, with an orange Ub-binding helix) in complex with Ub (blue) [PDB ID 3by4 (23)]. The inset shows the interaction of the Ub-binding helix with the Ub hydrophobic patch. (*D*) Superposition of vOTU–Ub and yOtul–Ub complexes shown in two orientations. Proteins are colored as in (*A*) and (*D*), and OTU domains are shown as semitransparent cartoon. The 75° rotation of Ub along the long helix of Ub is indicated in the right image.

A significant difference between Ub and ISG15 binding exists at a second interaction site. The hydrophobic helix of the helical arm of vOTU, including Pro77 and Leu81, interacts with a second hydrophobic patch in ISG15-C centered on Trp123 (that replaces Arg42 in Ub)(Fig. 3*B* and Fig. S2). Hence, ISG15 contains two adjacent hydrophobic surfaces that are contacted by vOTU (Fig. 3*B* and Fig. S2).

Pro130 (corresponding to Gln49 in Ub) bridges the two hydrophobic surfaces of ISG15-C and interacts with both the hydrophobic helix (Pro77 of vOTU) and with the N-terminal extension (Ile14 of vOTU). This allows a tighter packing of the ISG15-C β3-strand, which is up to 2.5 Å closer to the vOTU core compared to Ub. Overall, vOTU binding to ISG15 appears to be tighter compared to Ub, consistent with a 2–fold lower K_M for ISG15.

The N-Terminal Extension in vOTU Is Essential for Activity. As mentioned above, the N-terminal extension that shapes the S1 binding site is a unique feature of vOTU. Because the overall OTU domain fold would be maintained without this extension, we analyzed its importance for vOTU activity. A truncation variant of vOTU lacking the N-terminal 20 amino acids (vOTUΔN, residues 21–183) behaved similarly to vOTU and could be purified in large quantities from bacteria, indicating that removal of the N-terminus did not induce unfolding of the catalytic core. However, vOTU activity was significantly decreased when tested against both Ub-AMC and ISG15-AMC (Fig. 4 *A* and *B*), indicating that the N-terminal extension is essential for catalytic activity.

Viral OTU domains had previously been identified in Nairo- but also Arteriviruses (16). Nairoviruses including CCHFV contain an OTU domain at the very N-terminus of the L-protein. The N-terminus that forms the crucial vOTU extension is highly conserved in different Nairoviruses indicating similar structures and substrate binding modes of these OTU domains (Fig. 4*C* and Fig. S3).

In contrast, the OTU domain fold in arteriviruses such as equine arteritis virus (EAV) and porcine respiratory and reproductive syndrome virus, is preceded by additional folded protease domains (25). Strikingly, a region of similarity to the N-terminal extension in vOTU is present upstream of the EAV-nsp2 proteins (which comprises the OTU domain; Fig. S3). However, the autoproteolytic processing of the nsp1—nsp2 boundary facilitated by the nsp1 protease domain, removes the N-terminal extension in EAV (25) (Fig. S4). Hence, the processed EAV-nsp2 protein does not contain an N-terminal extension. EAV-nsp2 contains an insertion predicted to be in the helical arm of the OTU fold, which may be close to the S1 substrate binding site and may contribute to activity (Fig. S4). Structural studies of the EAV OTU domain will reveal how arterivirus OTU domains bind their substrates.

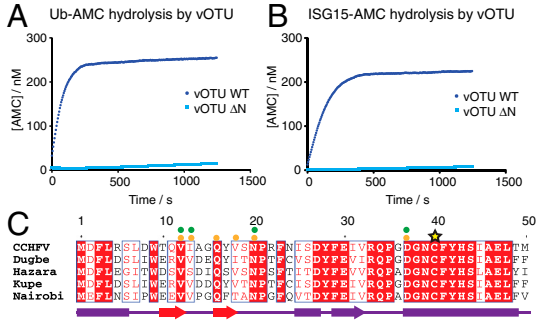

Fig. 4. The vOTU N-terminus is essential and conserved. (*A*) Ub-AMC assay of vOTU and vOTUΔN. (*B*) ISG15-AMC assay of vOTU and vOTUΔN. (*C*) Sequence alignment of the N-terminus in nairoviruses CCHFV (UniProt Accession number: Q6TQR6), Dugbe virus (Q66431), Hazara virus (A6XA53), Kupe virus (B8PWH5), and Nairobi sheep disease virus (D0PRM9). Alignments generated by the T-COFFEE server (http://www.ch.embnet.org/software/TCoffee.html) using regions corresponding to residues 1–183 (Fig. S3) of vOTU were visualized by ESPript 2.2 (http://espript.ibcp.fr/ESPript/ESPript/). Secondary structure elements are shown below the alignment. Residues contacting the Ub/ISG15 hydrophobic patch are indicated by orange or green dots, respectively, and a yellow star indicates the catalytic Cys residue.

Switching Substrate Specificity. Having identified the molecular determinants for cross-specificity in vOTU, we attempted to modulate the specificity of vOTU, to generate proteins that are specific for only one of the two modifiers. Apart from validating the observed binding modes in the complex structures, such mutant vOTU domains would be useful tools to study the relative contribution of ubiquitination vs. ISGylation in antiviral signaling pathways. Ub and ISG15-C interacted at the same site and in the same orientation, but displayed slightly distinct binding modes (Fig. 3*C* and Fig. S2). We reasoned that subtle mutations in vOTU that make use of the individual features of Ub or ISG15, could be sufficient to eliminate cross-reactivity in vOTU.

To abolish Ub-binding but keep ISG15-binding intact, we exploited the residue pair Ub Arg42/ISG15 Trp123 (Fig. 5 *A* and *B*). The positively charged Ub Arg42 interacts with vOTU Gln16 of the N-terminal extension, whereas ISG15 Trp123 is too far away for interactions with Gln16 (Fig. 5 *A* and *B*). We reasoned that a repelling positive charge at the Gln16 position [i.e., mutation to Arg (vOTU Q16R)], would specifically inhibit Ub interaction with little or no effect on ISG15 binding.

To generate a Ub-specific mutant vOTU, we exploited hydrophobic residues on the helical arm that interacted with ISG15 but not Ub (Fig. 5 *A* and *B*). Changing the hydrophobic nature of this helix would hence disrupt ISG15 binding but may not affect Ub binding. Pro77 at the center of this interface interacts

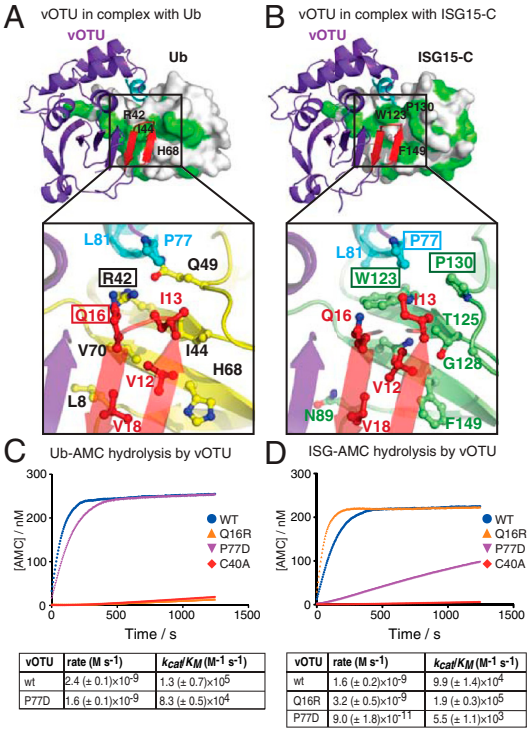

vOTU	rate (M s^{-1})	k_{cat}/K_M (M^{-1} s^{-1})
wt	2.4 (± 0.1)×10^{-9}	1.3 (± 0.7)×10^{5}
P77D	1.6 (± 0.1)×10^{-9}	8.3 (± 0.5)×10^{4}

vOTU	rate (M s^{-1})	k_{cat}/K_M (M^{-1} s^{-1})
wt	1.6 (± 0.2)×10^{-9}	9.9 (± 1.4)×10^{4}
Q16R	3.2 (± 0.5)×10^{-9}	1.9 (± 0.3)×10^{5}
P77D	9.0 (± 1.8)×10^{-11}	5.5 (± 1.1)×10^{3}

Fig. 5. Structural differences between Ub and ISG15 allow switching of vOTU specificity. (*A*) The top image shows Ub (under a surface with hydrophobic residues colored green) bound to vOTU centered on the N-terminal extension. Ile44 of Ub is indicated on the surface. The image below is a close-up of the interface between Ub (yellow) and vOTU, highlighting the interaction between vOTU Gln16 and Ub Arg42. (*B*) vOTU in complex with ISG15-C (green) depicted as in (*A*). Residues Trp123, Pro130, and Phe149 are indicated on the surface of ISG15-C. The image below centers on the vOTU Pro77 interaction with Pro130 and Trp123 of ISG15. (*C*) Ub-AMC assays for vOTU and mutants. (*D*) ISG15-AMC assays for vOTU and mutants.

with ISG15 Trp123 and Pro130 (Fig. 5*B*). We reasoned that mutation to Asp (vOTU P77D) would disfavor apolar interactions with Trp123 in ISG15, but may strengthen interaction with Arg42, the equivalent residue in Ub.

These mutations, alongside with a catalytically inactive mutant vOTU C40A, were tested in quantitative Ub/ISG15-AMC assays (Fig. 5 *C* and *D*). vOTU and vOTU C40A served as positive and negative control respectively. The vOTU P77D mutation retained Ub–AMC hydrolysis to a similar extent as vOTU (Fig. 5*C*), whereas its ability to hydrolyze ISG15-AMC was severely impaired (Fig. 5*D*). The specificity constant for this mutant is only slightly decreased (1.6-fold) for Ub–AMC hydrolysis, but ∼18-fold reduced for hydrolysis of ISG15–AMC. Even more strikingly, the vOTU Q16R mutant did not hydrolyze Ub–AMC (Fig. 5*C*), whereas hydrolysis of ISG15–AMC was increased 2-fold (Fig. 5*D*). We tested the generated vOTU mutants also against the panel of six diUb chains in qualitative DUB assays, confirming inactivity of vOTU Q16R, and showing that the Ub linkage-specificity had not been altered in any of the mutants (Fig. S5).

In a second type of analysis, we tested whether the vOTU mutants were able to interact with suicide inhibitors based on Ub (termed Ub*) or ISG15 (ISG15*)(Fig. 6*A*). For this, suicide probes were prepared as for crystallography, and used in analytical scale assays. Most of the input vOTU reacted with the suicide probe within 5 min, and enzymes or probes with reduced affinity showed less reactivity, generating a qualitative readout of substrate affinity. We observed Ub* reactivity for vOTU, and vOTU P77D (Fig. 6*A*, lanes 8 and 11), whereas the Ub* probe reacted significantly weaker with vOTU Q16R, vOTUΔN, or vOTU C40A (lanes 10, 9, and 12 in Fig. 6*A*). Likewise, an ISG15* probe reacted strongly with vOTU and vOTU Q16R (lanes 14 and 16), but was less reactive with vOTU P77D, vOTUΔN, or vOTU C40A (lanes 17, 15, and 18 in Fig. 6*A*). These results were consistent with the AMC assay, and demonstrated that we had separated the Ub and ISG15 specificities of vOTU.

Arg42/Trp123—A Critical Difference Between Ub and ISG15. The substrate-switching mutations in vOTU exploited the difference between a positively charged Arg42 in Ub and a bulky hydrophobic Trp123 in ISG15. Using mutated suicide probes, where Arg42 in Ub was mutated to Ala (Ub*R42A), or where Trp123 in ISG15 was mutated to Arg (ISG15*W123R), we could further confirm the specificity of our mutant vOTU domains (Fig. 6*B*). Both mutant probes modified vOTU significantly less compared to wild-type probes (lanes 7–10). Consistently, whereas Ub* reacted less well with vOTU Q16R compared to vOTU (lane 12), the Ub*R42A mutant probe now reacted strongly with the deubiquitinase-deficient vOTU Q16R mutant (lane 13). Furthermore, the ISG15*W123R mutant probe modified the vOTU Q16R mutant significantly less (lane 15), as both proteins now contain repelling positively charged residues at the interaction interface (Fig. 6*B*). Finally, Ub* R42A is less efficient in modifying vOTU P77D (lanes 17 and 18), showing that the vOTU P77D mutant indeed interacted with Arg42. However, an ISG15*W123R mutant probe did not show increased reactivity with the vOTU P77D mutant (lanes 19 and 20).

Validation of vOTU Mutant Specificity Against Cellular Substrates. The specificity of vOTU mutants was tested also against a polyubiquitinated model substrate, polyUb-UBE2S (18). Incubation with vOTU or vOTU P77D collapsed the high-molecular weight polyubiquitinated species to a visible ladder of smaller chains, whereas the vOTUΔN or vOTU Q16R mutant failed to hydrolyze Ub linkages in the substrate (Fig. 7*A*).

Finally, we tested the vOTU mutants against in vivo generated ISGylated substrates. Protein ISGylation was induced in HeLa cells by treatment with IFNβ (14), and HeLa cell lysates were incubated with vOTU, vOTUΔN, vOTU Q16R, and vOTU P77D, separated by SDS-PAGE and Western-blotted with an anti-ISG15 antibody to detected ISGylated proteins. As previously reported, vOTU could significantly reduce protein ISGylation in cell lysates (16). Consistent with our biochemical characterization, both the vOTUΔN mutant and the vOTU P77D mutant were impaired in deISGylation of substrates, whereas the vOTU Q16R mutant was as active as wild-type vOTU (Fig. 7*B*).

Overall, the biochemical characterization confirmed that we had successfully changed the substrate preference of a cross-specific DUB/deISGylase, to generate variants with specificity for either Ub (vOTU P77D) or ISG15 (vOTU Q16R).

Discussion

In this work, we characterized the OTU domain of CCHFV, a highly pathogenic human virus, and provided structural and functional insights into its activity as a DUB and deISGylase. Quantitative kinetic measurements revealed a slightly higher affinity of vOTU for ISG15. The kinetic parameters of vOTU show a significantly higher enzyme activity compared to pre-

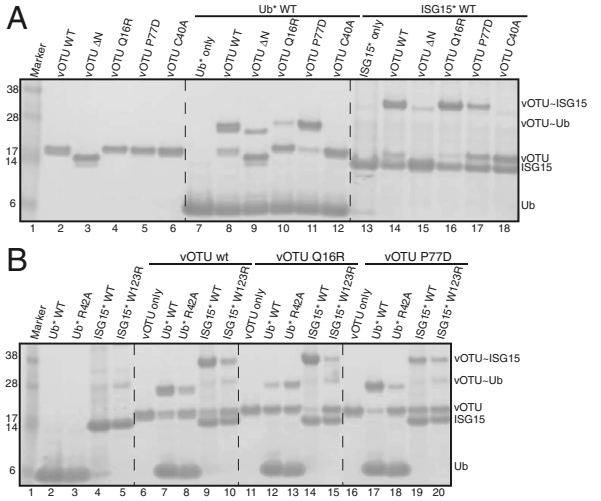

Fig. 6. Analysis of vOTU cross-reactivity using suicide probes. Ub and ISG15 thioesters were converted with 2-chloroethylamine hydrochloride to suicide inhibitors according to ref. 24, and tested against vOTU and vOTU mutants. Reactions were stopped after 5 min, resolved on SDS-PAGE gels and Coomassie stained. (*A*) Reaction of vOTU and mutants with Ub and ISG15 suicide probes. (*B*) Reaction of vOTU, vOTU Q16R, and vOTU P77D with Ub, Ub R42A, ISG15, and ISG15 W123R mutant suicide probes. WT; wild-type vOTU.

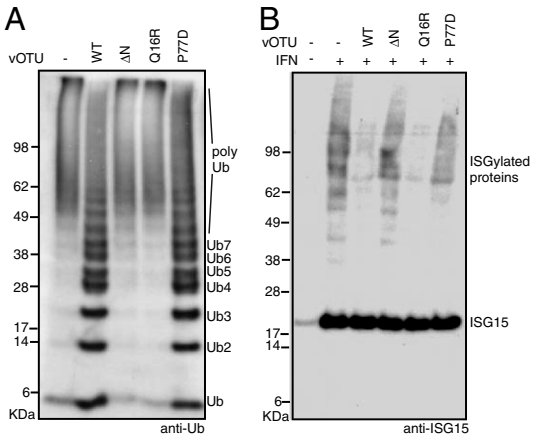

Fig. 7. Verification of vOTU mutant specificity against in vivo substrates. (*A*) PolyUb UBE2S was incubated with wild-type and mutant vOTU and ubiquitinated species were detected by Western blotting with an anti-Ub antibody (Millipore). (*B*) HeLa cells were stimulated with IFNβ according to ref. 14, and total cell lysates were incubated with vOTU and mutants. ISG15 was detected by Western blotting with an anti-ISG15 antibody (Santa Cruz). WT; wild-type vOTU.

viously studied human OTU family DUBs, such as TRABID (19) and yOtu1 (23), indicating that vOTU is a highly efficient enzyme.

ISG15 is thought to modify proteins as a monomer, in contrast to Ub, which forms eight distinct polymers in cells (4). Analysis of the intrinsic linkage specificity of vOTU against available diUb chains revealed the relative nonspecificity of vOTU that cleaved 4 out of 6 tested chain types, including K6-linkages that other OTU DUBs fail to hydrolyze (19). However, this analysis showed that vOTU is inefficient in cleaving linear and surprisingly also K29-linked chains. This suggests that hydrolysis of K29 or linear chains may not be essential for CCHFV to counteract the antiviral response. Interestingly, vOTU has been shown to release linear chains from the NF-κB essential modifier (NEMO) adaptor protein, where it had presumably targeted the isopeptide bond between NEMO and the first Ub (22). Alternatively, K29-linkages or linear chains may contribute in some way to viral replication and need to be maintained during infection.

The defined diUb cleavage profile of vOTU is an interesting addition to the recent characterization of linkage-specificity in human OTU DUBs, describing OTUB1 as a K48-specific enzyme (21), TRABID as a K29-specific enzyme (19), and Cezanne as a K11-specific enzyme (18). OTU family DUBs may become useful diagnostic tools in the analysis of Ub linkage types. Understanding the linkage specificity of OTU domains, however, will require complex structures with diUb bound across the active site, which has not been achieved.

Structural analysis of vOTU bound to Ub and ISG15 revealed the molecular basis for the observed cross-reactivity as well as unique features of viral OTU domains. The OTU domain fold in CCHFV and other Nairoviruses comprises additional N-terminal secondary structure elements that shape the S1 Ub/ISG15 binding site. These additional β-strands interact with the Ub hydrophobic patch, resulting in an intrinsic ∼75° rotation of Ub when compared to yOtu1–Ub (23), the only reported OTU–Ub complex structure to date. The plasticity of the S1 binding site is interesting, highlighting that further structural studies of OTU–Ub complexes are required. Although the 15 human OTU domain family members are not predicted to contain a similar N-terminal extension (8), this needs to be confirmed by structural analysis.

The first structure of vOTU bound to ISG15 revealed unique interaction properties of this antiviral Ub-like modifier. ISG15 interacted via two hydrophobic surfaces with complementary surfaces on vOTU, resulting in a 2-fold higher affinity (K_M) for ISG15. Notably, vOTU is slightly more active against Ub (k_{cat}), highlighting that both DUB and deISGylase activities are carefully balanced to contribute to vOTU function.

It will be exciting to see whether other ISG15-specific interactors exist that, like vOTU, utilize the two hydrophobic patches of ISG15. USP18/UBP43 is currently the only mammalian DUB known to hydrolyze ISG15 specifically (26), and PLpro, another viral DUB/deISGylase, has also been shown to have specificity for ISG15 (27). The molecular basis for specificity of these enzymes is still unknown.

It has become clear that many viruses dedicate effector proteins to counter protein ISGylation (13). However, the role of ISG15 in the antiviral response of host cells is still debated. Our reported mutants of vOTU may become important tools to study the relative contribution of ubiquitination vs. ISGylation in viral pathogenesis.

The distinct structural features of the CCHFV vOTU compared to human OTU domains may be exploited in structure-based inhibitor design. An inhibitor for CCHFV vOTU would not directly interfere with viral replication (28), but may enable the innate immune system to efficiently target the pathogen. Our structural characterization of vOTU provides a foundation for such future studies, and may result in treatments for CCHF and related diseases.

Materials and Methods

Detailed experimental procedures can be found in *SI Text, Materials and Methods*. vOTU cDNA was obtained by gene synthesis (Gene Ltd.) and vOTU proteins were expressed as glutathione S-transferase fusions in *E. coli*. Thioester-derivatives of Ub and ISG15 were converted into suicide probes with 2-chloroethylamine hydrochloride according to ref. 24. Crystallographic data were collected at the European Synchrotron Radiation Facility (ESRF) and Diamond Light Source synchrotrons (Table S1 and Fig. S6). DiUb generation, fluorescence anisotropy and AMC assays were performed according to ref. 19 and are described in detail in *SI Text, Materials and Methods*.

Coordinates and structure factors have been deposited with the protein data bank, accession codes 3PHU, 3PHW, and 3PHX.

ACKNOWLEDGMENTS. We thank Y. Kulathu, A. Bremm, and M. Hospenthal for reagents, help with experiments, and discussions, and M. Bienz and F. Randow for comments on the manuscript. We thank Keith D. Wilkinson for the gift of Ub and ISG15 intein constructs. M.A. and S.V. are Medical Research Council (MRC) Career Development Fellows.

1. Akira S, Uematsu S, Takeuchi O (2006) Pathogen recognition and innate immunity. *Cell* 124:783–801.
2. O'Neill LA, Bowie AG (2010) Sensing and signaling in antiviral innate immunity. *Curr Biol* 20:R328–333.
3. Sadler AJ, Williams BRG (2008) Interferon-inducible antiviral effectors. *Nat Rev Immunol* 8:559–568.
4. Komander D (2009) The emerging complexity of protein ubiquitination. *Biochem Soc Trans* 37:937–953.
5. Zeng W, et al. (2010) Reconstitution of the RIG-I pathway reveals a signaling role of unanchored polyubiquitin chains in innate immunity. *Cell* 141:315–330.
6. Skaug B, Jiang X, Chen ZJ (2009) The role of ubiquitin in NF-kappaB regulatory pathways. *Annu Rev Biochem* 78:769–796.
7. Tokunaga F, et al. (2009) Involvement of linear polyubiquitylation of NEMO in NF-kappaB activation. *Nat Cell Biol* 11:123–132.
8. Komander D, Clague MJ, Urbé S (2009) Breaking the chains: Structure and function of the deubiquitinases. *Nat Rev Mol Cell Biol* 10:550–563.
9. Wertz I, et al. (2004) De-ubiquitination and ubiquitin ligase domains of A20 downregulate NF-kappaB signalling. *Nature* 430:694–699.
10. Kayagaki N, et al. (2007) DUBA: A deubiquitinase that regulates type I interferon production. *Science* 318:1628–1632.
11. Dao CT, Zhang DE (2005) ISG15: A ubiquitin-like enigma. *Front Biosci* 10:2701–2722.
12. Narasimhan J, et al. (2005) Crystal structure of the interferon-induced ubiquitin-like protein ISG15. *J Biol Chem* 280:27356–27365.
13. Skaug B, Chen ZJ (2010) Emerging role of ISG15 in antiviral immunity. *Cell* 143:187–190.
14. Durfee LA, Lyon N, Seo K, Huibregtse JM (2010) The ISG15 conjugation system broadly targets newly synthesized proteins: implications for the antiviral function of ISG15. *Mol Cell* 38:722–732.
15. Randow F, Lehner PJ (2009) Viral avoidance and exploitation of the ubiquitin system. *Nat Cell Biol* 11:527–534.
16. Frias-Staheli N, et al. (2007) Ovarian tumor domain-containing viral proteases evade ubiquitin- and ISG15-dependent innate immune responses. *Cell Host Microbe* 2:404–416.
17. Weber F, Mirazimi A (2008) Interferon and cytokine responses to Crimean Congo hemorrhagic fever virus; an emerging and neglected viral zonoosis. *Cytokine Growth F R* 19:395–404.
18. Bremm A, Freund SM, Komander D (2010) Lys11-linked ubiquitin chains adopt compact conformations and are preferentially hydrolyzed by the deubiquitinase Cezanne. *Nat Struct Mol Biol* 17:939–947.
19. Virdee S, Ye Y, Nguyen DP, Komander D, Chin JW (2010) Engineered diubiquitin synthesis reveals Lys29-isopeptide specificity of an OTU deubiquitinase. *Nat Chem Biol* 6:750–757.
20. Komander D, et al. (2009) Molecular discrimination of structurally equivalent Lys 63-linked and linear polyubiquitin chains. *EMBO Rep* 10:466–473.
21. Edelmann MJ, et al. (2009) Structural basis and specificity of human otubain 1-mediated deubiquitination. *Biochem J* 418:379–390.
22. Xia Z-P, et al. (2009) Direct activation of protein kinases by unanchored polyubiquitin chains. *Nature* 461:114–119.
23. Messick TE, et al. (2008) Structural basis for ubiquitin recognition by the Otu1 ovarian tumor domain protein. *J Biol Chem* 283:11038–11049.
24. Borodovsky A, et al. (2002) Chemistry-based functional proteomics reveals novel members of the deubiquitinating enzyme family. *Chem Biol* 9:1149–1159.
25. Ziebuhr J, Snijder EJ, Gorbalenya AE (2000) Virus-encoded proteinases and proteolytic processing inthe Nidovirales. *J Gen Virol* 81:853–879.
26. Malakhov MP, Malakhova OA, Kim KI, Ritchie KJ, Zhang DE (2002) UBP43 (USP18) specifically removes ISG15 from conjugated proteins. *J Biol Chem* 277:9976–9981.
27. Lindner HA, et al. (2007) Selectivity in ISG15 and ubiquitin recognition by the SARS coronavirus papain-like protease. *Arch Biochem Biophys* 466:8–14.
28. Bergeron E, Albarino CG, Khristova ML, Nichol ST (2009) Crimean-Congo hemorrhagic fever virus-encoded ovarian tumor protease activity is dispensable for virus RNA polymerase function. *J Virol* 84:216–226.